A pangenome graph reference of 30 chicken genomes allows genotyping of large and complex structural variants

Edward Rice, Antton Alberdi, James Alfieri, Giridhar Athrey, Jennifer Balacco, Philippe Bardou, Heath Blackmon, Mathieu Charles, Hans Cheng, Olivier Fedrigo, et al.

A pangenome graph reference of 30 chicken genomes allows genotyping of large and complex structural variants

Edward S. Rice
Antton Alberdi
James Alfieri
Giridhar Athrey
Jennifer R. Balacco
Philippe Bardou
Heath Blackmon
Mathieu Charles
Hans H. Cheng
Olivier Fedrigo
Steven R. Fiddaman
Giulio Formenti
Laurent Frantz
M. Thomas P. Gilbert
Cari J. Hearn
Erich D. Jarvis
Christophe Klopp
Sofia Marcos
Deborah Velez-Irizarry
Luohao Xu
Wesley C. Warren (warrenwc@missouri.edu)

Research Article

Keywords: Gallus gallus, K locus, IGLL1, ev21

Posted Date: June 21st, 2023

DOI: https://doi.org/10.21203/rs.3.rs-3086064/v1

A pangenome graph reference of 30 chicken genomes allows genotyping of large and complex structural variants.

Edward S. Rice[1,2], Antton Alberdi[3], James Alfieri[4], Giridhar Athrey[5], Jennifer R. Balacco[6], Philippe Bardou[7], Heath Blackmon[8], Mathieu Charles[9], Hans H. Cheng[10], Olivier Fedrigo[6], Steven R. Fiddaman[11], Giulio Formenti[6], Laurent Frantz[2,12], M. Thomas P. Gilbert[3], Cari J. Hearn[10], Erich D. Jarvis[6,13], Christophe Klopp[14], Sofia Marcos[3,15], Deborah Velez-Irizarry[10], Luohao Xu[16], Wesley C. Warren[17]*

[1] Bond Life Sciences Center, University of Missouri, Columbia, MO, USA
[2] Faculty of Veterinary Medicine, Ludwig-Maximilians-Universität, München, Germany
[3] Center for Evolutionary Hologenomics, Globe Institute, University of Copenhagen (UCPH), Copenhagen, Denmark
[4] Department of Ecology & Evolutionary Biology, Texas A&M University, College Station, TX, USA
[5] Department of Poultry Science, Texas A&M University, College Station, TX, USA
[6] Vertebrate Genome Laboratory, The Rockefeller University, New York, NY, USA
[7] Sigenae, GenPhySE, Université de Toulouse, INRAE, ENVT, F-31326, Castanet Tolosan, France
[8] Department of Biology, Texas A&M University, College Station, TX, USA
[9] INRA Centre de Toulouse Midi-Pyrénées: Castanet Tolosan, Midi-Pyrénées, FR
[10] USDA, ARS, USNPRC, Avian Disease and Oncology Laboratory, East Lansing, MI, USA
[11] Department of Biology, University of Oxford, OX1 3SZ, UK
[12] School of Biological and Behavioural Sciences, Queen Mary University of London, London E1 4DQ, UK
[13] The Howard Hughes Medical Institute, Chevy Chase, MD, USA
[14] Sigenae, Genotoul Bioinfo, MIAT UR875, INRAE, Castanet Tolosan, France
[15] Applied Genomics and Bioinformatics, University of the Basque Country (UPV/EHU), Leioa, Bilbao, Spain
[16] Key Laboratory of Freshwater Fish Reproduction and Development (Ministry of Education), Key Laboratory of Aquatic Science of Chongqing, School of Life Sciences, Southwest University, Chongqing 400715, China
[17] Department of Animal Sciences, University of Missouri, Columbia, MO, USA

* To whom correspondence should be addressed: warrenwc@missouri.edu

Keywords (at least 3): Gallus gallus, K locus, IGLL1, ev21

Abstract

Background. The red junglefowl, the wild progenitor of domestic chickens, has historically served as a reference for genomic studies of domestic chickens. These studies have provided insight into the etiology of traits of commercial importance. However, the use of a single reference genome does not capture diversity present among modern breeds, many of which have accumulated molecular changes due to drift and selection. While reference-based resequencing is well-suited to cataloging simple variants such as single nucleotide changes and short insertions and deletions, it is mostly inadequate to discover more complex structural variation in the genome.

Results. We present a pangenome for the domestic chicken consisting of thirty assemblies of chickens from different breeds and research lines. We demonstrate how this pangenome can be used to catalog structural variants present in modern breeds and untangle complex nested variation. We show that alignment of short reads from 100 diverse wild and domestic chickens to this pangenome reduces reference bias by 38%, which affects downstream genotyping results. This approach also allows for the accurate genotyping of a large and complex pair of structural variants at the K 'feathering' locus using short reads, which would not be possible using a linear reference.

Conclusions. We expect that this new paradigm of genomic reference will allow better pinpointing of exact mutations responsible for specific phenotypes, which will in turn be necessary for breeding chickens that meet new sustainability criteria and are resilient to quickly evolving pathogen threats.

Introduction

Accurately detecting sequence variation associated with traits of economic importance in the domestic chicken is a major goal of genetic research into this globally widespread dietary protein source [1]. Many groups are now genotyping chicken genomes to discover the underlying molecular basis of specific traits [2–6], but current methods, both sequence- and array-based, have unquantified limitations in assessing the underlying variation that connects many loci to studied traits. Investigations in other species into the variant sets compiled by techniques relying on existing linear references have revealed large gaps in variation discovery ability [7–10]. For the domestic chicken, improved completeness and accuracy of bioinformatic queries into this variation are of vital importance to the field, as computational experiments are rapidly becoming the venue of choice to assess the potential of artificial selection to improve qualities such as growth, nutrient digestibility, reproduction, and perhaps most importantly, immune resilience.

Current frequently employed methods for genotyping whole genomes mostly share the core strategy of aligning short reads to a reference genome derived from a single individual [11]; these references are usually compressed haploid representations of diploid genomes, with toggling of haplotypes due to haploid compression, or chimeric haploblocks due to allele mixing [12,13]. While these methods, given a reference genome of sufficient quality and reads of sufficient coverage, are able to capture most single nucleotide variants (SNVs) and small insertions and deletions (indels) in populations, they can lead to reference bias [14,15], and they consistently underestimate all types of structural variants (SVs) [8]. Furthermore, for best performance, the most accurate genotyping software [16] requires preexisting high-quality data about the distribution of polymorphic sites

throughout the genome for statistical calibration [17] or model training [18], information that does not exist for most species. Large-scale long-read resequencing can mitigate some of these limitations [19], but the high cost and low accuracy of long reads compared to short reads, and the large amount of existing publicly available short-read sequencing data — for chicken, there are over 40,000 short read data sets on the SRA at the time of writing but fewer than 500 long read experiments — make a full transition to the use of long reads for resequencing studies unlikely in the near future.

The limitations of these approximations have led to the evolution of methods in the detection of SVs [7]. Over the past decade, many algorithms have been developed to detect these segregating and de novo SVs using short-read approaches [20]. The association of these SVs with traits has been undeniable but usually overlooked in favor of the more straightforward use of single nucleotide variants (SNVs) in GWAS studies [20]. The best-performing of these algorithms can detect around 11,000 SVs in humans, but face significant problems with both false positives and false negatives [7]. In contrast, when using long-read methodologies, this detection threshold nearly doubles [10,21]. In chicken, several studies have called SVs or copy number variants (CNVs) using the aforementioned short read algorithms [22,23], but each lacks an understanding of how SV detection could be limited by not only the short reads used but also the reference to which sequences are aligned. In these studies and others, content is not only missed but falsely called, with no regional genomic context in how this variation is best classified.

To counter these limitations, several methods have been developed to create and use pangenome graphs as references [24–28]. A pangenome graph is a data structure that encodes the sequence and variation present among the genomes of multiple individuals [29]. While a linear

97 reference usually contains only the sequence of a single individual, a pangenome includes sequence
98 common to all individuals as well as information about the position, alleles, and frequencies of each
99 variant site. The recent publication of a draft pangenome for human demonstrated that this new
100 paradigm allows recovery of much sequence that appears with nonnegligible frequency in the genomes
101 of individuals across the species but is missing from even the telomere-to-telomere linear reference
102 [30].

103 An additional advantage of cataloging variation in the form of a pangenome instead of a list of
104 variants relative to a linear reference is that a pangenome can represent nested variation. For example, if
105 multiple non-reference individuals have an insertion, but the insertion happened far enough in the
106 past that the inserted sequence now contains segregating SNVs, variant calls against a linear reference
107 would treat each version of the insertion as an independent allele, while a pangenome shows the
108 variant as a single insertion containing additional nested variation within it. By contrast, a linear
109 representation of this variant would consider each possible path through the insertion as a separate
110 allele, rather than breaking it down into a single biallelic presence/absence variant along with a series of
111 smaller variants nested within the presence allele sequence. Furthermore, reads containing no reference
112 sequence can map to the insertion, whereas when aligning to a linear reference, such reads would either
113 remain unaligned, or, even worse, map to a different location in the genome with similar sequence.

114 Alignment of short reads to a pangenome reference instead of a linear reference has been
115 demonstrated in humans and other species, including birds, to recapitulate and improve downstream
116 genotype calling accuracy for both small variants (i.e., SNPs and small indels) and larger structural
117 variants [9,31,32]. Large insertions are nearly uncallable when using short-reads aligned to linear

118 references, with the recall of tools such as Delly [33] falling to zero for insertions larger than 400bp,
119 while graph-based tools such as VG and paragraph [25] are mostly unaffected by variant length [31].
120 The human pangenome's demonstrations of improvements in read mapping, small variant
121 genotyping, novel variant discovery, SV genotyping, and representation of complex variants [30] show
122 the potential of this new paradigm for genome references.
123 In chicken, multiple alignments of reference-guided short-read assemblies [34] and *de novo*
124 assemblies of high-error PacBio CLR reads [35] have revealed sequences present among chickens
125 worldwide but missing from current references, as well as other previously unknown SVs. However,
126 although these whole-genome alignments were both described as pangenomes by their respective
127 authors, neither study generated a pangenome graph that can be used by other researchers as a
128 reference for alignment to overcome the limitations presented by reference bias and difficulty in
129 capturing SVs. They are further limited by their reliance on short reads or low-accuracy long reads,
130 respectively, for assembly.
131 In this study, we use current best practices to generate a pangenome graph of 30 highly
132 continuous genome assemblies of various chicken breeds, including broilers, layers, and research lines.
133 We use this pangenome to catalog variation present in the input assemblies, including variation that
134 was not detectable in studies using other methods, focussing on SVs in an immune system gene and a
135 feathering-related locus as illustrations. We then go on to align short reads from 100 chickens to the
136 graph, showing the improved performance of this method for alignment accuracy and genotyping
137 recall compared to linear reference alignment. We expect that adoption of this new resource will allow
138 better results in genotyping in future studies, with a goal to move toward more effective uses of

chicken genome references and in the process significantly improve researchers' ability to discover the molecular mechanisms that determine bird healthiness.

Results

Selection of chromosome-level assemblies

To build assembly-based pangenome references, we used the five most continuous chromosome-level assemblies of the domestic chicken currently available, along with alternate haplotypes as applicable, and new contig-level assemblies of thirteen additional chickens, most of them resolved into haplotypes. These chromosome-level assemblies have contig N50 values ranging from 5.47 to 91.3 Mb (see Table 1). This includes the current species reference assembly on NCBI RefSeq, bGalGal1b, also known as GRCg7b (contig N50 = 18.8 Mb), a haplotype-resolved assembly of a commercial broiler line created using the trio-binning method and an F1 cross between a representative commercial broiler and a white leghorn layer [36]. bGalGal1b, as the current RefSeq reference assembly, is fully annotated, so we use it as the source of annotations in this study. Because this assembly was made using trio-binning, its creation also resulted in a haplotype-resolved assembly of the genetic contribution of the other parent, a white leghorn layer. We refer to this assembly as bGalGal1w, and it is also known as GRCg7w and we use both assemblies in our pangenome.

We sequenced and assembled to the chromosome level the genomes of two additional broilers from the Ross (Aviagen) and Cobb (Cobb-Vantress) lines, to capture more of the diversity present among commercial lines of domestic chickens, and to take advantage of advances in sequencing that have occurred since the assembly of bGalGal1b and bGalGal1w, especially base-calling improvements

in PacBio's HiFi/Circular Consensus Sequence (CCS) technology. HiFi reads are accurate enough to allow the hifiasm algorithm to assemble contigs for both haplotypes [37], so although we only assembled the primary contigs into chromosomes, we used the alternate contigs during pangenome construction as well to take full advantage of their individual haploid diversity.

We also integrated the first nearly complete assembly of a chicken [38]. This assembly is of a Huxu, a Chinese broiler breed, and we refer to it as "huxu".

Finally, we sequenced and assembled both haplotypes of 13 additional chickens to a contig level using HiFi sequencing (Supplemental table 1). These chickens include research lines bred to study immune function as well as domestic breeds originating in Spain and Egypt. We produced sequencing coverage of at least 25x (mean 35x) for each bird based on a genome size of 1.1Gb. We successfully assembled both haplotypes of 10 out of 13 birds into contigs, and used partially phased primary contig assemblies of the remaining 3, resulting in a total of 23 assemblies with a minimum contig N50 of 11 Mb (mean 15 Mb).

Together, these 30 assemblies represent a diverse set of domestic chickens, including commercial lines, research lines, and broiler and layer breeds originating on three continents. They also were assembled using three different techniques: haplotype-resolved trio-binning of the F1 offspring of a cross between two breeds (bGalGal1b and bGalGal1w), HiFi haplotype-resolved assembly (bGalGal4, bGalGal5, and additional chickens), and the current best-practice de novo assembly technique using a combination of HiFi and Oxford Nanopore Ultralong (ONT UL) reads (huxu) [38]. While collectively these genomes do not come close to fully capturing the diversity of domestic

chickens worldwide, they provide a good working template of a first pangenome reference of the domestic chicken genome.

ID	Assembled bird	Accession	Ref	Contig N50 (Mb)
bGalGal1b	Commercial broiler	GCA_016699485.1	[36]	18.8
bGalGal1w	White leghorn layer	GCA_016700215.2	[36]	17.7
bGalGal4	Ross broiler	GCA_027557775.1	N/A	5.47
bGalGal5	Cobb broiler	GCA_027408225.1	N/A	8.33
HuxuT2T	Huxu broiler	GCA_024206055.1	[38]	91.3

Table 1: The five chromosome-level assemblies used as a base for creation of pangenome references for the domestic chicken.

Creation of pangenome references

We constructed pangenome references of the chicken genome using two different methods, both used by the Human Pangenome Reference Consortium [30]: PanGenome Graph Builder (PGGB) [30] and minigraph-cactus [39]. PGGB and minigraph-cactus both take multiple assemblies as input, perform whole-genome alignments on them, and derive a pangenome graph from these alignments. We made a preliminary graph using each method and five chromosome-level assemblies (Table 1). For minigraph-cactus, we then created a 30-assembly graph using these five chromosome-level assemblies as well as the contig-level alternate haplotype assemblies of bGalGal4 and bGalGal5 and assemblies of both haplotypes of thirteen additional chickens from HiFi data (Supplementary Table 1). We did not create a 30-assembly graph with PGGB due to the computational intractability of the 5-assembly PGGB graph for downstream applications, as described below. Therefore, the final two graphs we tested were the 5-assembly PGGB graph and the 30-assembly minigraph-cactus graph.

196 The minigraph-cactus pangenome graph contains 49 million nodes and 67 million edges, and
197 therefore a mean degree, or the number of edges attached to a node, of 1.4. The total length of
198 sequence represented in the graph is 1.13 Gb. The combined length of nodes traversed by the most
199 complete assembly, Huxu, is 1.02 Gb. This is smaller than the 1.10 Gb total size of the assembly. This
200 difference is because a path can traverse the same sequence in the graph multiple times, for example, in
201 the case of a duplication. Therefore, there is in total 0.11 Gb (9.9%) of additional sequence in the
202 graph compared to the length of the most complete assembly. Of the other assemblies, bGalGal1b
203 contributes the most additional sequence, 55.6 Mb, to the graph, while some assemblies contribute as
204 little as 200 kb of additional sequence as a result of their relatedness to others (Supplementary Figure
205 S1).
206 The PGGB pangenome graph contains 33 million nodes and 45 million edges, and therefore
207 also a mean degree of 1.4. We found that parameter choice had a large effect on the numbers of nodes
208 and edges, as well as the maximum degree, although not the mean degree (Supplementary Figure S2).
209 Despite this pangenome being made up of only five assemblies instead of 30, it contains more
210 sequence than the minigraph-cactus pangenome: the total length of sequence represented in the
211 PGGB graph is 1.23 Gb, an additional 147 Mb or 12.0% of sequence compared to the total length of
212 graph nodes in the Huxu genome (1.09 Gb).
213 The 109 Mb of additional sequence is closer to previous estimates of total variation in diverse
214 groups of chickens [40–43] than 147 Mb, suggesting overestimation by PGGB. Comparative
215 examination of graph structures revealed that much of the additional sequence in the PGGB graph is
216 likely due to regions of assemblies that are homologous but were not properly aligned by the pipeline,

causing large bubbles and loose ends in the graph (Supplementary Figure S3). Another source of additional sequence in this graph is duplications that are treated as simple insertions, leading to the same sequence occurring twice in the graph; one example of this occurs in the K locus, which we discuss below. For these reasons, we used only the minigraph-cactus graph for most subsequent analyses.

Cataloging of variants present in input assemblies

A pangenome graph contains the variation present in the input assemblies, and can thus be used to genotype the input assemblies compared to one chosen as a reference, based on deviations from this reference path. We chose bGalGal1b for the reference as it is the highest-quality RefSeq-annotated chicken reference genome currently available. In total, we found 15 million variants present in at least one of the other 29 haplotypes compared to bGalGal1b. 12 million of these variants are SNVs (Figure 1a). This is a smaller number of total SNVs than has been detected in large panel studies [42,43], which is likely a result of the smaller sample size of our experiment, with 30 haplotypes compared to 678 in [42]. We found a similar total length of deleted sequence, 19.2 Mb, as a previous study based on long read alignments, 19.7 Mb [41]. However, we were able to recover 18.5 Mb of inserted sequence, while the previous study recovered only 6.74 Mb [41] (Figure 1a). Although distributions of lengths of deletions found previously by read alignment and by our pangenome method were broadly similar, we found more long insertions than was possible with long-read alignment (Figure 1b).

237 The B cell receptor gene *IGLL1*, which has been used as a marker for plasma B cells in chicken
238 [44], contains examples of these different kinds of variation. The overall structure of the pangenome
239 graph of *IGLL1* shows that there are many small variants, as well as two SVs (Figure 2). By encoding
240 the presence of small variants and their allele frequencies into the reference (Figure 2a), alignment to
241 pangenomes has been shown to reduce reference bias compared to a linear reference [24], which we
242 confirm below for our chicken pangenome. For example, for the SNV shown in Figure 2a, short reads
243 containing the non-reference allele are in less danger of mapping incorrectly as the aligner is aware of
244 the 17% chance of an A in this position of the genome.
245 The larger of the two SVs in the pangenome graph of *IGLL1* is a ~5kb deletion relative to
246 bGalGal1b present in only one haplotype of one chicken, UCD312 (Figure 2b). By recording this low-
247 frequency deletion in the reference, the pangenome method ensures that reads from resequenced
248 chickens containing the deletion are able to map to both flanking sequences through edge e1 without
249 splitting, which would introduce a potential source of error.
250 Finally, a ~300bp insertion relative to bGalGal1b demonstrates how a pangenome graph is able
251 to losslessly represent nested variation (Figure 2c). The SNVs and indels within the inserted sequence
252 are encoded in the exact same way as they would be in reference sequence, giving a full picture of the
253 variation present in this region.
254
255 *Disentangling a tandem repeat and viral insertion at the K locus*
256 The K locus, short for "short wing" (*kürzer Flügel*), is a region of chrZ with an early feathering
257 (EF) allele and a late feathering (LF) allele [45,46]. The EF allele contains single copies of the genes

PRLR and *SPEF2*. The LF allele contains a tandem duplication of parts of both genes [47], and often, but not always [48,49], an insertion of the sequence of the avian leukosis virus ev21. The reference genome bGalGal1b has the EF allele and no ev21 insertion, so genotyping the K locus in other chickens using this reference is difficult as ev21 has a length of 9,679 bp [49], an order of magnitude longer than the maximum insertion size that can be genotyped with short reads and a linear reference [31]. As such, it is a region that can be more accurately genotyped with the use of a pangenome graph approach.

We first created a one-dimensional representation of the minigraph-cactus pangenome graph structure of the K locus colored by path coverage, as a node through which the same haplotype path travels more than once indicates a duplication (Figure 3a). This representation shows that while most of the haplotypes represented in the pangenome graph contain only one copy of this locus, Huxu has a duplicated region and an insertion. The 2x path coverage region in Huxu covers parts of both *PRLR* and *SPEF2*, consistent with the tandem duplication found by Elferink et al. [47]. We also found a misassembly in bGalGal1w, with unassigned scaffolds containing the sequence (see Supplementary Note 1 and Supplementary Figure S4). Furthermore, Huxu contains an insertion relative to the reference sequence bGalGal1b. Alignment verified that the inserted sequence is the ev21 genome.

Next, to better understand the structure of the locus, we created a two-dimensional representation of the graph at this locus (Figure 3b-d). This representation of the graph shows the tandem duplication as a junction where a path can either leave the K locus or repeat it (Figure 3c), and the insertion as a loop containing the ev21 genome covered only by Huxu (Figure 3d).

Finally, to view the alleles linearly, we used the "untangle" function of ODGI to lay out each haplotype (Figure 3e). The resulting gene layout of the two alleles is consistent with previous knowledge about the structure of the locus [47–49].

Repeating this process using the PGGB graph, we found that the PGGB graph did not contain the ev21 insertion, and treated the tandem duplication as a simple insertion rather than a duplication. Given the dependence of the PGGB output on good parameter choices, and previous demonstrations that PGGB graphs of small complex regions such as the human MHC can accurately reconstruct the structure of these loci, we hypothesize that choosing parameters specific to the level of divergence present at complex loci is necessary for PGGB to accurately reconstruct them.

Use as a reference for resequencing and genotyping

Given the improvements in accuracy and recall of genotyping shown in other species by using pangenome graph-based methods, we set out to demonstrate the usefulness of our pangenome representations for alignment and genotyping. For this, we used simulated short reads as well as short reads from 100 domestic and wild chickens (Supplementary Table 2). For comparison between linear and graph-based methods, we called genotypes using both linear alignments to bGalGal1b as well as graph alignments to our pangenomes.

For downstream use by existing short-read genotype callers, alignments must be converted from graph coordinates to linear coordinates; this process is called surjection. Alignment of short reads to the PGGB graph and surjection to bGalGal1b was infeasible, with a throughput of only 1.6 reads per CPU-second on a test set of 10k paired-end reads, and inability to complete alignment of a larger

test set of 1M paired-end reads without running out of memory with 250 GB allocated to the job. Further investigation revealed that surjection was the bottleneck, as graph alignment without subsequent surjection had a throughput of 147 reads per CPU-second and a maximum memory usage of 31GB for the 1M test set. By comparison, alignment of the 1M test set to the minigraph-cactus graph followed by surjection to bGalGal1b had a throughput of 500 reads per CPU-second and a maximum memory usage of 24GB, and minimap2 could align 1832 reads per CPU-second to bGalGal1b with 5.4 GB memory (Figure 4a-b).

In order to compare accuracy of graph alignment to linear alignment, we simulated one million pairs of paired-end reads and aligned them to both the cactus-minigraph pangenome with VG giraffe and the linear bGalGal1b reference with minimap2. Giraffe performed better than minimap at every level of stringency, based on what percentage of all reads were mapped correctly (Figure 4c).

To test the downstream effects of these differences in mapping accuracy, we genotyped 100 chickens from diverse breeds using both giraffe pangenome alignments and minimap linear alignments of 10-15x coverage short reads, and compared the results between the two methods (Figure 5). While the two methods found similar sets of SNVs (Figure 5a) and indels (Figure 5b), there were substantial differences. Agreement was unsurprisingly higher for SNVs, although the pipeline using giraffe alignments found a larger number with a quality score of at least 10 than the pipeline using minimap (Figure 5a). For variants found by both methods, per-sample SNV concordance had a mean of 97.9% with a standard deviation of 9.1% (Figure 5c). Indel concordance was lower, with a mean of 94.0% and a standard deviation of 12.9% (Figure 5d).

To determine whether reference bias is a factor in the different genotyping results between the two methods, we examined the proportion of mapped reads containing the reference allele at putative heterozygous SNV sites. Reference bias across these sites, which we define as the difference between the mean fraction of reads containing the alternate allele and the expected alternate allele fraction of 0.5, is lower for all of the 100 chickens when using pangenome alignment instead of linear alignment, with a mean reference bias reduction of 38% (Figure 5e, Supplementary Figure S5).

Finally, we used the short read alignments to the pangenome graph to genotype the K locus based on edge coverage (Figure 5f). All of these chickens are female and thus only have one copy of the Z-linked K locus. Of the 100 chickens, 23 have the ev21 insertion (ev21+) and 24 have the tandem repeat (late feathering/LF). As found in previous studies [48,49], the ev21 insertion and the tandem duplication are not inextricably linked, although they do usually appear together: three chickens, all standard Rhode Island breeds, have the ev21 insertion but not the tandem repeat, and four chickens, two Silkies and two Cochins, have the tandem repeat but not the ev21 insertion.

Discussion

With the quickly accumulating numbers of haplotype-resolved genomes for many species, the pangenome model of integrated presentation of within-species variation stands to become ubiquitous [29,30]. Such resources already exist for other livestock such as swine [50] and cattle [51,52]. One of the greatest advantages of pangenome references in other species has been the capture of sequences not present in linear reference genomes. Compared to the nearly complete assembly of the Huxu chicken genome, our pangenome graph contains 109 Mb of additional sequence. Some of this additional

sequence comes from SNVs or small indels that are relatively straightforward to represent in the context of a linear reference, and some of it is made up of nodes whose sequences are similar to nodes traversed by the Huxu assembly, but are represented separately. Thus, the true accessory genome length is likely less than 109 Mb compared to Huxu. Nonetheless, the tripling of total insertion length detectable using this pangenome compared to long read alignments shows that much of this additional sequence is made up of variation that cannot be represented in a traditional linear reference genome, and therefore, many reads from these regions of the genome cannot be mapped to a linear reference as it does not contain the parts of the genome the reads came from. By adding additional assembled chicken genomes of more diverse origins this amount of novel sequence will grow.

While other studies have presented multiple alignments of chickens as pangenomes [34,35], our graph-based approach, which uses assemblies based on long and highly accurate PacBio HiFi reads as well as one near-complete assembly, allows the pangenome to be used not just as a method for cataloging variation present in the input assemblies, but also as a reference for future resequencing studies. By comparing pipelines using linear versus pangenome alignments of short reads to genotype 100 chickens from diverse breeds, we demonstrated the improved alignment performance of pangenome alignment over linear alignment, and showed the downstream effects of these improvements on genotyping. Unfortunately, there does not yet exist a high-confidence truth set of variant calls for chickens as there does for humans [16], so we cannot compare the accuracy of these differing genotype calls. Nonetheless, given the improvements in alignment performance we have shown in chicken with both simulated and real reads, and the improvements in genotyping demonstrated in human and yeast by using the giraffe pangenome aligner [9,30], we predict that the

361 genotypes we inferred using giraffe pangenome alignment are substantially more accurate than those
362 we inferred using linear alignment.
363 Our determination of the structure of the K locus and subsequent genotyping demonstrates
364 the power of pangenome graphs in the study of loci containing complex structural variants. The initial
365 discovery of the insertion of an endogenous avian leukosis virus in the late feathering allele required
366 cell culture work [53], and a later study establishing the tandem repeat [47] necessitated extensive
367 quantitative PCR experiments targeted at 20 different segments of the locus. Although the latter was
368 performed after a linear reference genome was available, this reference, like all subsequent versions of
369 the reference genome for chicken, contains the early feathering allele and no ev21 insertion at the K
370 locus, and no current method can reliably genotype SVs of this size using short reads and a linear
371 reference [31]. More recent work on the relationship between the ev21 insertion and the late
372 feathering phenotype, though undertaken after improved reference genomes and large amounts of
373 public sequencing data from different breeds of chickens became available, also relied on targeted
374 PCR [48,49]. In contrast, we were able to replicate these findings using only existing short-read whole
375 genome sequencing data and pangenome methods. We expect that our pangenome, and future
376 pangenomes using telomere-to-telomere genome assemblies, which exist for increasing numbers of
377 species [54–58] but not yet chickens, will enable discoveries about complex structural variation at
378 important immune loci such as the major histocompatibility complex (MHC) and T cell receptor gene
379 (TCR), providing insight into the genetic diversity necessary to fight evolving pathogen threats in this
380 major worldwide source of protein, which also threaten wildlife with increasing frequency [59].

The current best-performing pangenome-based SV calling pipeline [9] surjects graph alignments to linear coordinates, losing information in the process, and uses proprietary hardware and software optimized for human data. Thus, at this stage we did not attempt to genotype all SVs in the chickens with short-read data. Given the lack of ground truth SV data in chickens, we focussed on a single locus that has already undergone targeted genotyping from a wide variety of chicken breeds, and were able to confirm previous knowledge of the combinations of alleles present at this locus. We look forward to the development of open-source SV calling pipelines that perform well on non-human genomes and take full advantage of the information present in graph alignments.

Conclusions

In this paper, we have presented the first pangenome graph reference for the domestic chicken. We show its utility as a catalog of variation, including structural variation too large or complex to be detected using previous methods, and as a reference for the alignment of short reads. Given the improvements we have demonstrated in this model over a linear reference, we expect this pangenome, and new versions with additional broadly diverse chicken breeds incorporated, to serve as a resource to the community for future resequencing studies as well as investigation of complex loci, especially in immune-related genes.

Methods

Sequencing and assembly of bGalGal4 and bGalGal5

401 One female Ross 308 (Aviagen) and one female Cobb 550 (Cobb-Vantress), both commercial
402 broiler chickens, were euthanized in the framework of a research experiment at 38 days of age. Cardiac
403 puncture was immediately employed to collect 12 aliquots of 100 ul of blood in tubes with EDTA and
404 1 ml of ethanol >99.7% from each animal. Samples were frozen at -20 °C.
405 For both assemblies (bGalGal4 and bGalGal5), we followed the VGP 2.0 pipeline [12]. We
406 generated 32x Pacbio HiFi data on a Sequel IIe, and then used cutadapt [60] to trim off adapters that
407 were not trimmed in the Pacbio software processing. We assembled contigs using HiFiasm v0.14 [61],
408 generating a semi-haplotyped phased primary contig and alternate contig assembly. From the primary
409 assembly, we removed false haplotype duplication and placed them in the alternate using purge_dups
410 v1.2.5 [62]. We then scaffolded the contigs with Bionano Genomics optical maps (319x and 459x
411 respectively), generated on a Saphyr instrument using DLE label, with Bionano Solve. We then further
412 scaffolded with Arima Genomics Hi-C v2 (65x and 122x respectively), using salsa v2.2 [63]. The
413 primary assembly was then curated using gEVAL [64], structural errors corrected, and chromosomes
414 named according to their numbers in the bGalGal1 GRC7g reference. 10X Genomics data were also
415 generated, and used for orthogonal validation, but not scaffolding. The primary and alternate
416 assemblies were deposited in NCBI under accession numbers GCA_027557775.1 (bGalGal4) and
417 GCA_027408465.1 (bGalGal5), and all data are available in Genome Ark
418 https://genomeark.github.io/genomeark-all/Gallus_gallus/.
419
420 *Sequencing and assembly of additional chickens*

High molecular weight (HMW) DNA from blood of 13 juvenile male chickens (Supplementary Table 1), maintained and bled under ADOL IACUC-approved Animal Use Protocol #2019-15 for breeder management, was sequenced on the Pacific BioSciences Sequel IIe. HMW samples were sheared using a Diagenode Megarupter3 shearing device targeting 18-22KB fragments. Libraries were prepared with the PacBio SMRTbell Prep Kit 3.0. Library size distribution was determined on the Agilent Femto Pulse and a Qubit fluorometer was used to measure concentration. Sequencing polymerase was bound to the SMRTbell libraries with the Binding Kit 3.2, and run on Sequel IIe with the Sequel II Sequencing Kit 2.0 and SMRT Cell 8M. HiFi data was collected with Instrument Control Software Version 11.0 and Chemistry Bundle 11.0 with a movie time of 30 hours. The On Plate Loading Concentration was 130pmolar.

HiFi reads for each of the chickens were assembled into contigs using hifiasm v0.18.9 [37] with default options. Both haplotypes output by hifiasm were used in subsequent analyses.

Creation of PGGB pangenome

We constructed a pangenome reference from the five input assemblies bGalGal1b, bGalGal1w, bGalGal4, bGalGal5, and HuxuT2T (Table "assemblies"). First, we extracted chromosome sequences from the assemblies and gave them names according to the PanSN-spec, in the format of "[assembly name]#[chromosome name]", e.g., "bGalGal4#chr5". We partitioned the assemblies into 41 communities, one for each chromosome, and then constructed a pangenome graph for each chromosome separately. Due to disagreements in the naming of microchromosomes among

441 the five assemblies, some of the communities contain chromosomes named differently in the different
442 assemblies (Supplementary Table 3).
443 For every chromosome, we constructed its pangenome graph using the Pangenome Graph
444 Builder (PGGB) v0.4.1 [30]. Briefly, this pipeline uses wfmash v0.9.1 [65] to align the input
445 assemblies, seqwish v0.7.6 [28] to build a graph from the alignments, smoothxg v0.6.5 [66] and gfaffix
446 v0.1.3 [67] to clean up the graph, and odgi v0.7.3 [27] to visualize the graph. We first ran pggb with
447 default parameters, except for parameter "-n" set to the number of assemblies being aligned for the
448 chromosome in question (this number is five for most chromosomes, with the exception of sex
449 chromosomes and some microchromosomes without full representation in all five assemblies) and "-G
450 3079,3559". For postprocessing and optimal visualization, we redrew the 2D graph visualization using
451 the odgi draw command with parameters "-C -w1000", and we redrew the 1D graph visualization by
452 first resorting the graph based on positions in the bGalGal5 path using the command odgi sort with
453 parameters '-H <(echo "bGalGal5#${chromosome_name}") -Y' and then drawing with the odgi viz
454 command with default parameters.
455 To find the optimal parameters for each chromosome, we performed a parameter sweep of the
456 segment length (-s), mapping percent identity (-p), and minimum match length (-k) options to the
457 pggb command. We tested every member of the cartesian product set of the parameter values s={5k,
458 10k, 30k, 50k, 80k}, p={85, 90, 94,97}, and k={10, 19, 50, 100, 150}. We evaluated the results as
459 suggested in PGGB documentation, using a combination of examination of graph statistics, especially
460 node count and maximum degree, with the odgi stats command and visual inspection of the graph
461 structure using the odgi viz output. For some microchromosomes, we made more granular

adjustments to the parameters to fine-tune their graphs. Supplementary Table 3 shows the final parameters chosen for each chromosome.

Finally, we created a single pangenome graph containing the respective connected component for each community using the odgi squeeze command with default parameters. This resulted in a single graph file with extension ".og" that is easily convertible to other sequence graph formats such as GFA and VG.

Creation of minigraph-cactus pangenome

We ran the minigraph-cactus pipeline [39] using the cactus v2.4.2 Docker image and a nextflow pipeline built for this purpose [68]. As input, we used the five chromosome-level assemblies in Table 1, the alternate haplotypes of bGalGal4 and bGalGal5, and both haplotype assemblies of an additional 13 chickens listed in Supplementary Table 1. We specified bGalGal1b as the reference, because although it is not the highest-quality assembly, it is the best RefSeq-annotated assembly on NCBI, so we wanted to call variants against it downstream.

Additional sequence analysis

We determined the amount of additional sequence contributed to the graph by each sample through an iterative process. First, we removed all nodes traversed by the Huxu assembly from the graph as it is the most complete assembly. Then, for each remaining bird, we summed up the length of all nodes traversed by either haplotype of this bird, found the bird with the largest sum, and removed all nodes traversed by this bird's haplotypes from the graph. We repeated this process until there were

no samples remaining. The python program we wrote for this purpose is included in the repository cited in the Code Availability statement.

Format conversions and subgraph extraction

To convert GFAv1.1 format as output by minigraph-cactus to OG format, we used the command "vg convert -gfW" to convert to GFAv1.0, and then "odgi build -g -Os" to build an OG graph out of the GFAv1.0 file.

To convert GBZ format to HG format, we used the command "vg convert".

To convert HG format to GFA format, we used the command "vg convert -f".

To convert OG format to GFA format, we used the command "odgi view -a -g".

To extract regions from graphs in HG format, we used the command "vg find -p 'bGalGal1b#[chromosome]:[start]-[end]'".

To extract regions from graphs in OG format, we used the command "odgi extract -d0 -E -r 'bGalGal1b#[chromosome]:[start]-[end]'".

Genotyping input assemblies

Both assembly-based graph construction pipelines, pggb and minigraph-cactus, can output vcf files containing genotypes for the input assemblies relative to the reference, in our case bGalGal1b. Minigraph-cactus does this by default; pggb does with the addition of the option "-V 'bGalGal1b:#:'". Where necessary, we concatenated vcf files for each chromosome into a single genome-wide vcf using the bcftools concat command v1.15.1 [69].

Graph visualization

To visualize specific regions of the pangenome graph, we first looked up coordinates relative to bGalGal1b on RefSeq, extracted them from the graph, output in GFA format, and visualized using bandage v0.8.1 [70]. Commands for extraction and conversion are given under the heading "Format conversions and subgraph extraction."

Read simulation

We simulated reads using the "vg sim" command with a nucleotide substitution error rate of 0.24% as estimated by Pfeiffer et al. [71] and an indel error rate of 0.029% as in [9].

Sequencing of short read chickens

We sampled 236 chickens from 62 breeding farms that specialize in heritage and rare chicken breeds in May and December 2021. In short, we collected 0.5 - 2 mL of blood from each bird by puncturing the brachial vein with a syringe (gauge size 18.5 - 28 depending on the size of the bird). The blood was immediately expelled through the syringe into K2EDTA vacutainers and stored on dry ice. Upon arrival at the lab, the blood samples were transferred to a -80 C freezer. DNA was extracted using the QIAamp Fast DNA Tissue Kit. Library preparation and sequencing were performed at BGI Group. Libraries were prepared using a DNA short-insert protocol for 150 bp paired-end reads and sequenced on the DNBseq platform. 7 samples failed to be sequenced due to low quality, so were excluded from further analyses. We chose a subset of 100 of these samples for the final analysis.

Short read alignment

To align short reads to the PGGB graph, we first converted the graph to GFA format using the command "odgi view -g" and then converted the GFA format to GBZ format [72] and created giraffe indices from the output with the command "vg autoindex -w giraffe". The minigraph-cactus pipeline outputs all indices necessary to run giraffe by default, so no further processing was necessary to prepare it for alignment of reads with giraffe.

To test timing and memory usage, we arbitrarily chose a publicly available set of short reads from a chicken (SRR9967588) and subsetted the first 1 million pairs. This test failed for alignment to the PGGB graph due to running out of memory, but a smaller subset of 10,000 read pairs was successful. We aligned the test set of reads to the graph using the command "vg giraffe" with arguments "-o BAM". Because the PGGB graph does not contain a reference sequence like the minigraph-cactus graph, we additionally specified the reference chromosomes with the arguments "--ref-paths bGalGal1b_paths.tsv", where bGalGal1b_paths.tsv is a tab-separated file containing a list of all chromosomes in bGalGal1b and their sizes. For comparison to alignment to a linear reference with minimap2 v2.24 [73], we created a short-read minimap index of bGalGal1b with the command "minimap2 -x sr -d" and then aligned reads to it with the command "minimap2 -a" piped to "samtools view -bh" with samtools v1.16.1 [69] to convert to bam format for a fair comparison, since we ran giraffe with bam output.

For alignment of short reads from 100 chickens, we ran vg giraffe with default options, outputting the results in GAM format. We surjected the GAM files to BAM format with bGalGal1b as the reference genome using the command “vg surject” with default options.

Comparison of linear and graph alignments with simulated reads

To compare the accuracy of alignments of simulated reads between linear and graph aligners, we aligned the simulated reads both to the bGalGal1b linear reference using minimap2 and to the pangenome graph reference using giraffe, as described above. We converted the minimap2 output to GAM format using the command “vg inject”, and then compared the minimap2 and giraffe GAMs to the truth set using “vg gamcompare”, all as in [9].

Genotyping

We genotyped the 100 chickens based on these alignments using elprep [74] v5.1.2, a multithreaded reimplementation of GATK. Briefly, we generated an elfasta sequence reference for bGalGal1b using the command “elprep fasta-to-elfasta”, created a list of sites from the minigraph-cactus vcf output with SVs larger than 1000bp filtered out using the command “elprep vcf-to-elsites”, and ran the “sfm” command with settings as recommended in the manual to generate a gvcf for each bird, which we then combined into a single gvcf with GATK CombineGVCFs and joint genotyped with GATK GenotypeGVCFs [17]. The location of our scripts for genotyping, as well as all other analyses in this paper, is given in the Data Availability section.

Genotyping method comparison

To compare the respective outputs of the giraffe- and minimap-based genotyping pipelines, we used bcftools v1.17 [69] command "isec -c some" to create four vcf files: variants only detected by the giraffe pipeline, variants only detected by the minimap pipeline, giraffe pipeline calls of variants detected by both pipelines, and minimap pipeline calls of variants detected by both pipelines. We counted variants with QUAL>=10 in all of these files, subsetting by variant type with "bcftools view -v [snp|indel]". To compare the per-sample calls made by the respective methods for variants detected by both, we used "bcftools merge --force-samples" to create a single vcf containing calls made by both methods, and then used a custom python script (included in code availability) to calculate the percent agreement for each variant.

Reference bias estimation

We estimated the amount of reference bias by calculating the mean fraction of reads mapping to putative heterozygous sites containing the alternate allele, and comparing to the expected value of 0.5. We define putative heterozygous sites as positions with coverage of at least 10x where the portion of reads containing the minor allele is at least 25%, as in [15]. Briefly, we filtered low-quality mappings and multimapping reads with "samtools view -F2304 -q10", created pileups with "samtools mpileup -d100 –no-BAQ", and piped the results to a custom C program to find putative heterozygous sites and calculate alternate allele frequencies at these sites. All code used to perform this analysis is in the project's code repository.

K locus genotyping

To genotype the K locus, we converted each GAM file to GAF format using the command "vg convert -G" and counted reads covering the edges e1 through e7 as shown in Figure "K locus". We used binomial tests with p-value cutoffs of 0.05 to assign genotypes to each chicken for both the ev21 insertion and the tandem duplication; chickens with both p(insertion) > 0.05 and p(no insertion) > 0.05 were marked as inconclusive.

Declarations

Ethics approval and consent to participate

Chickens used for the bGalGal4 and bGalGal5 assemblies were euthanized according to the procedures regulated in the Spanish Royal Decree RD 53/2013. Experimentation procedures were approved by the Ethical Committee of Generalitat de Catalunya, Spain (Proceeding number 10226).

Chickens used for additional assemblies were maintained and bled under ADOL IACUC-approved Animal Use Protocol #2019-15 for breeder management. SPF birds from each line were grown in colony cages and provided food and water *ad libitum*.

For chickens used for short read sequencing, all handling and sample collection of animals were performed in accordance with TAMU AUP 2022-0091.

Consent for publication

Not applicable.

Availability of data and materials

606 The datasets generated and/or analyzed in the current study are available in NCBI repositories
607 under BioProject accessions PRJNA838369, PRJNA838370, and PRJNA971225. The pangenome
608 graph, a vcf of variants present in the graph, and vcfs of the resequenced chickens genotyped using
609 both linear and pangenome methods are available in a Zenodo repository at [embargoed until final
610 publication]. The code used to perform the analysis in the current study is available on GitHub at
611 https://github.com/WarrenLab/chicken-pangenome-paper.

612 *Competing interests*

613 The authors declare that they have no competing interests.

614 *Funding*

615 This work was supported by USDA NIFA grants 2020-67015-31574 and 2022-67015-36218
616 and the European Union's Horizon Research and Innovation Programme under grant agreement No.
617 817729 (Project HoloFood). Computation for this work was performed on the high performance
618 computing infrastructure provided by Research Computing Support Services and in part by the
619 National Science Foundation under grant number CNS-1429294 at the University of Missouri,
620 Columbia MO. The authors gratefully acknowledge the Gauss Centre for Supercomputing e.V.
621 (www.gauss-centre.eu) for funding this project by providing computing time on the GCS
622 Supercomputer SuperMUC-NG at Leibniz Supercomputing Centre (www.lrz.de).

623 *Authors' contributions*

624 WCW and ESR conceived and designed the project. AA, JA, GA, HB, HHC, MTPG, CJH,
625 SM, and DV generated sequence data used in this project. ESR, JRB, OF, GF, EDJ, and LX assembled
626 genomes used to create the pangenome. ESR, PB, MC, SRF, LF, and CK genotyped chickens used in

this project. ESR constructed the pangenome. ESR and WCW wrote the manuscript. All authors edited and approved the manuscript.

Acknowledgements

Not applicable.

633 **References**

634 1. Athrey G. Chapter 18 - Poultry genetics and breeding. In: Bazer FW, Lamb GC, Wu G, editors.
635 Animal Agriculture. Academic Press; 2020. p. 317–30.

636 2. Drobik-Czwarno W, Wolc A, Fulton JE, Arango J, Jankowski T, O'Sullivan NP, et al. Identifying
637 the genetic basis for resistance to avian influenza in commercial egg layer chickens. Animal.
638 2018;12:1363–71.

639 3. Xu L, He Y, Ding Y, Liu GE, Zhang H, Cheng HH, et al. Genetic assessment of inbred chicken
640 lines indicates genomic signatures of resistance to Marek's disease. J Anim Sci Biotechnol. 2018;9:65.

641 4. Wang Q, Li D, Guo A, Li M, Li L, Zhou J, et al. Whole-genome resequencing of Dulong Chicken
642 reveal signatures of selection. Br Poult Sci. 2020;61:624–31.

643 5. Seifi Moroudi R, Ansari Mahyari S, Vaez Torshizi R, Lanjanian H, Masoudi-Nejad A.
644 Identification of new genes and quantitative trait locis associated with growth curve parameters in F2
645 chicken population using genome-wide association study. Anim Genet. 2021;52:171–84.

646 6. Perlas A, Argilaguet J, Bertran K, Sánchez-González R, Nofrarías M, Valle R, et al. Dual Host and
647 Pathogen RNA-Seq Analysis Unravels Chicken Genes Potentially Involved in Resistance to Highly
648 Pathogenic Avian Influenza Virus Infection. Front Immunol. 2021;12:800188.

649 7. Zhao X, Collins RL, Lee W-P, Weber AM, Jun Y, Zhu Q, et al. Expectations and blind spots for
650 structural variation detection from long-read assemblies and short-read genome sequencing
651 technologies. Am J Hum Genet. Elsevier; 2021;108:919–28.

652 8. Mahmoud M, Gobet N, Cruz-Dávalos DI, Mounier N, Dessimoz C, Sedlazeck FJ. Structural
653 variant calling: the long and the short of it. Genome Biol. 2019;20:246.

654 9. Sirén J, Monlong J, Chang X, Novak AM, Eizenga JM, Markello C, et al. Pangenomics enables
655 genotyping of known structural variants in 5202 diverse genomes. Science. 2021;374:abg8871.

656 10. Audano PA, Sulovari A, Graves-Lindsay TA, Cantsilieris S, Sorensen M, Welch AE, et al.
657 Characterizing the Major Structural Variant Alleles of the Human Genome. Cell. 2019;176:663–
658 75.e19.

659 11. Nielsen R, Paul JS, Albrechtsen A, Song YS. Genotype and SNP calling from next-generation
660 sequencing data. Nat Rev Genet. 2011;12:443–51.

661 12. Rhie A, McCarthy SA, Fedrigo O, Damas J, Formenti G, Koren S, et al. Towards complete and
662 error-free genome assemblies of all vertebrate species. Nature. 2021;592:737–46.

663 13. Ko BJ, Lee C, Kim J, Rhie A, Yoo DA, Howe K, et al. Widespread false gene gains caused by
664 duplication errors in genome assemblies. Genome Biol. 2022;23:205.

665 14. Brandt DYC, Aguiar VRC, Bitarello BD, Nunes K, Goudet J, Meyer D. Mapping Bias
666 Overestimates Reference Allele Frequencies at the HLA Genes in the 1000 Genomes Project Phase I
667 Data. G3 . 2015;5:931–41.

668 15. Günther T, Nettelblad C. The presence and impact of reference bias on population genomic
669 studies of prehistoric human populations. PLoS Genet. 2019;15:e1008302.

670 16. Barbitoff YA, Abasov R, Tvorogova VE, Glotov AS, Predeus AV. Systematic benchmark of state-
671 of-the-art variant calling pipelines identifies major factors affecting accuracy of coding sequence
672 variant discovery. BMC Genomics. 2022;23:155.

673 17. Van der Auwera GA, O'Connor BD. Genomics in the Cloud: Using Docker, GATK, and WDL in
674 Terra. "O'Reilly Media, Inc."; 2020.

675 18. Poplin R, Chang P-C, Alexander D, Schwartz S, Colthurst T, Ku A, et al. A universal SNP and
676 small-indel variant caller using deep neural networks. Nat Biotechnol. 2018;36:983–7.

677 19. De Coster W, Weissensteiner MH, Sedlazeck FJ. Towards population-scale long-read sequencing.
678 Nat Rev Genet. 2021;22:572–87.

679 20. Chiang C, Scott AJ, Davis JR, Tsang EK, Li X, Kim Y, et al. The impact of structural variation on
680 human gene expression. Nat Genet. 2017;49:692–9.

681 21. Chaisson MJP, Sanders AD, Zhao X, Malhotra A, Porubsky D, Rausch T, et al. Multi-platform
682 discovery of haplotype-resolved structural variation in human genomes. Nat Commun. Nature
683 Publishing Group; 2019;10:1–16.

684 22. Rao YS, Li J, Zhang R, Lin XR, Xu JG, Xie L, et al. Copy number variation identification and
685 analysis of the chicken genome using a 60K SNP BeadChip. Poult Sci. 2016;95:1750–6.

686 23. Weng Z, Xu Y, Li W, Chen J, Zhong M, Zhong F, et al. Genomic variations and signatures of
687 selection in Wuhua yellow chicken. PLoS [Internet]. journals.plos.org; 2020; Available from:
688 https://journals.plos.org/plosone/article?id=10.1371/journal.pone.0241137

689 24. Garrison E, Sirén J, Novak AM, Hickey G, Eizenga JM, Dawson ET, et al. Variation graph toolkit
690 improves read mapping by representing genetic variation in the reference. Nat Biotechnol.
691 2018;36:875–9.

692 25. Chen S, Krusche P, Dolzhenko E, Sherman RM, Petrovski R, Schlesinger F, et al. Paragraph: a
693 graph-based structural variant genotyper for short-read sequence data. Genome Biol. BioMed Central;
694 2019;20:1–13.

695 26. Li H, Feng X, Chu C. The design and construction of reference pangenome graphs with
696 minigraph. Genome Biol. BioMed Central; 2020;21:265.

697 27. Guarracino A, Heumos S, Nahnsen S, Prins P, Garrison E. ODGI: understanding pangenome
698 graphs. Bioinformatics. 2022;38:3319–26.

699 28. Garrison E, Guarracino A. Unbiased pangenome graphs. Bioinformatics. Oxford Academic;
700 2022;39:btac743.

701 29. Eizenga JM, Novak AM, Sibbesen JA, Heumos S, Ghaffaari A, Hickey G, et al. Pangenome
702 Graphs. Annu Rev Genomics Hum Genet. 2020;21:139–62.

703 30. Liao W-W, Asri M, Ebler J, Doerr D, Haukness M, Hickey G, et al. A Draft Human Pangenome
704 Reference. Nature. 2023;617:312–24.

705 31. Hickey G, Heller D, Monlong J, Sibbesen JA, Sirén J, Eizenga J, et al. Genotyping structural
706 variants in pangenome graphs using the vg toolkit. Genome Biol. 2020;21:35.

707 32. Secomandi S, Gallo GR, Sozzoni M, Iannucci A, Galati E, Abueg L, et al. A chromosome-level
708 reference genome and pangenome for barn swallow population genomics. Cell Rep. 2023;42:111992.

709 33. Rausch T, Zichner T, Schlattl A, Stütz AM, Benes V, Korbel JO. DELLY: structural variant
710 discovery by integrated paired-end and split-read analysis. Bioinformatics. 2012;28:i333–9.

711 34. Wang K, Hu H, Tian Y, Li J, Scheben A, Zhang C, et al. The Chicken Pan-Genome Reveals Gene
712 Content Variation and a Promoter Region Deletion in IGF2BP1 Affecting Body Size. Mol Biol Evol.
713 2021;38:5066–81.

714 35. Li M, Sun C, Xu N, Bian P, Tian X, Wang X, et al. De Novo Assembly of 20 Chicken Genomes
715 Reveals the Undetectable Phenomenon for Thousands of Core Genes on Microchromosomes and
716 Subtelomeric Regions. Mol Biol Evol [Internet]. 2022;39. Available from:
717 http://dx.doi.org/10.1093/molbev/msac066

718 36. Smith J, Alfieri JM, Anthony N, Arensburger P, Athrey GN, Balacco J, et al. Fourth Report on
719 Chicken Genes and Chromosomes 2022. Cytogenet Genome Res [Internet]. 2023; Available from:
720 http://dx.doi.org/10.1159/000529376

721 37. Cheng H, Jarvis ED, Fedrigo O, Koepfli K-P, Urban L, Gemmell NJ, et al. Haplotype-resolved
722 assembly of diploid genomes without parental data. Nat Biotechnol. 2022;40:1332–5.

723 38. Huang Z, Xu Z, Bai H, Huang Y, Kang N, Ding X, et al. Evolutionary analysis of a complete
724 chicken genome. Proc Natl Acad Sci U S A. 2023;120:e2216641120.

725 39. Hickey G, Monlong J, Ebler J, Novak AM, Eizenga JM, Gao Y, et al. Pangenome graph

726 construction from genome alignments with Minigraph-Cactus. Nat Biotechnol [Internet]. 2023;
727 Available from: http://dx.doi.org/10.1038/s41587-023-01793-w

728 40. Li D, Li Y, Li M, Che T, Tian S, Chen B, et al. Population genomics identifies patterns of genetic
729 diversity and selection in chicken. BMC Genomics. 2019;20:263.

730 41. Zhang J, Nie C, Li X, Zhao X, Jia Y, Han J, et al. Comprehensive analysis of structural variants in
731 chickens using PacBio sequencing. Front Genet. 2022;13:971588.

732 42. Liu R, Xing S, Wang J, Zheng M, Cui H, Crooijmans RPMA, et al. A new chicken 55K SNP
733 genotyping array. BMC Genomics. 2019;20:410.

734 43. Malomane DK, Simianer H, Weigend A, Reimer C, Schmitt AO, Weigend S. The SYNBREED
735 chicken diversity panel: a global resource to assess chicken diversity at high genomic resolution. BMC
736 Genomics. 2019;20:345.

737 44. Warren WC, Rice ES, Meyer A, Hearn CJ, Steep A, Hunt HD, et al. The immune cell landscape
738 and response of Marek's disease resistant and susceptible chickens infected with Marek's disease virus.
739 Sci Rep. 2023;13:5355.

740 45. Hertwig P, Rittershaus T. Die Erbfaktoren der Haushühner. Z Indukt Abstamm Vererbungsl.
741 1929;51:354–72.

742 46. Siegel PB, Mueller CD, Craig JV. Some Phenotypic Differences Among Homozygous,
743 Heterozygous, and Hemizygous Late Feathering Chicks1,2. Poult Sci. 1957;36:232–9.

744 47. Elferink MG, Vallée AAA, Jungerius AP, Crooijmans RPMA, Groenen MAM. Partial duplication
745 of the PRLR and SPEF2 genes at the late feathering locus in chicken. BMC Genomics. 2008;9:391.

746 48. Takenouchi A, Toshishige M, Ito N, Tsudzuki M. Endogenous viral gene ev21 is not responsible
747 for the expression of late feathering in chickens. Poult Sci. 2018;97:403–11.

748 49. Zhang X, Wang H, Zhang L, Wang Q, Du X, Ge L, et al. Analysis of a genetic factors contributing
749 to feathering phenotype in chickens. Poult Sci. 2018;97:3405–13.

750 50. Jiang Y-F, Wang S, Wang C-L, Xu R-H, Wang W-W, Jiang Y, et al. Pangenome obtained by long-
751 read sequencing of 11 genomes reveal hidden functional structural variants in pigs. iScience.
752 2023;26:106119.

753 51. Zhou Y, Yang L, Han X, Han J, Hu Y, Li F, et al. Assembly of a pangenome for global cattle reveals
754 missing sequences and novel structural variations, providing new insights into their diversity and
755 evolutionary history. Genome Res. 2022;32:1585–601.

756 52. Leonard AS, Crysnanto D, Mapel XM, Bhati M, Pausch H. Graph construction method impacts

variation representation and analyses in a bovine super-pangenome. Genome Biol. 2023;24:124.

53. Bacon LD, Smith E, Crittenden LB, Havenstein GB. Association of the slow feathering (K) and an endogenous viral (ev21) gene on the Z chromosome of chickens. Poult Sci. Elsevier; 1988;67:191–7.

54. Nurk S, Koren S, Rhie A, Rautiainen M, Bzikadze AV, Mikheenko A, et al. The complete sequence of a human genome. Science. 2022;376:44–53.

55. Rautiainen M, Nurk S, Walenz BP, Logsdon GA, Porubsky D, Rhie A, et al. Telomere-to-telomere assembly of diploid chromosomes with Verkko. Nat Biotechnol [Internet]. 2023; Available from: http://dx.doi.org/10.1038/s41587-023-01662-6

56. Xue L, Gao Y, Wu M, Tian T, Fan H, Huang Y, et al. Telomere-to-telomere assembly of a fish Y chromosome reveals the origin of a young sex chromosome pair. Genome Biol. 2021;22:203.

57. Belser C, Baurens F-C, Noel B, Martin G, Cruaud C, Istace B, et al. Telomere-to-telomere gapless chromosomes of banana using nanopore sequencing. Commun Biol. 2021;4:1047.

58. Bliznina A, Masunaga A, Mansfield MJ, Tan Y, Liu AW, West C, et al. Telomere-to-telomere assembly of the genome of an individual Oikopleura dioica from Okinawa using Nanopore-based sequencing. BMC Genomics. 2021;22:222.

59. Stokstad E. Deadly bird flu establishes a foothold in North America. Science. 2022;377:912–912.

60. Martin M. Cutadapt removes adapter sequences from high-throughput sequencing reads. EMBnet.journal. 2011;17:10–2.

61. Cheng H, Concepcion GT, Feng X, Zhang H, Li H. Haplotype-resolved de novo assembly using phased assembly graphs with hifiasm. Nat Methods. 2021;18:170–5.

62. Guan D, McCarthy SA, Wood J, Howe K, Wang Y, Durbin R. Identifying and removing haplotypic duplication in primary genome assemblies. Bioinformatics. 2020;36:2896–8.

63. Ghurye J, Pop M, Koren S, Bickhart D, Chin C-S. Scaffolding of long read assemblies using long range contact information. BMC Genomics. BioMed Central; 2017;18:527.

64. Chow W, Brugger K, Caccamo M, Sealy I, Torrance J, Howe K. gEVAL - a web-based browser for evaluating genome assemblies. Bioinformatics. 2016;32:2508–10.

65. Marco-Sola S, Moure JC, Moreto M, Espinosa A. Fast gap-affine pairwise alignment using the wavefront algorithm. Bioinformatics [Internet]. academic.oup.com; 2021; Available from: https://academic.oup.com/bioinformatics/article-abstract/37/4/456/5904262

66. smoothxg: linearize and simplify variation graphs using blocked partial order alignment [Internet].

787 Github; [cited 2023 Mar 9]. Available from: https://github.com/pangenome/smoothxg

788 67. GFAffix: GFAffix identifies walk-preserving shared affixes in variation graphs and collapses them
789 into a non-redundant graph structure [Internet]. Github; [cited 2023 Mar 9]. Available from:
790 https://github.com/marschall-lab/GFAffix

791 68. minigraph-cactus-nf: a nextflow pipeline for creating a pangenome with minigraph-cactus
792 [Internet]. Github; [cited 2023 Mar 10]. Available from: https://github.com/WarrenLab/minigraph-
793 cactus-nf

794 69. Danecek P, Bonfield JK, Liddle J, Marshall J, Ohan V, Pollard MO, et al. Twelve years of
795 SAMtools and BCFtools. Gigascience [Internet]. 2021;10. Available from:
796 http://dx.doi.org/10.1093/gigascience/giab008

797 70. Wick RR, Schultz MB, Zobel J, Holt KE. Bandage: interactive visualization of de novo genome
798 assemblies. Bioinformatics. 2015;31:3350–2.

799 71. Pfeiffer F, Gröber C, Blank M, Händler K, Beyer M, Schultze JL, et al. Systematic evaluation of
800 error rates and causes in short samples in next-generation sequencing. Sci Rep. 2018;8:10950.

801 72. Sirén J, Paten B. GBZ file format for pangenome graphs. Bioinformatics. 2022;38:5012–8.

802 73. Li H. Minimap2: pairwise alignment for nucleotide sequences. Bioinformatics. 2018;34:3094–
803 100.

804 74. Herzeel C, Costanza P, Decap D, Fostier J, Wuyts R, Verachtert W. Multithreaded variant calling
805 in elPrep 5. PLoS One. 2021;16:e0244471.

806

807

Figures

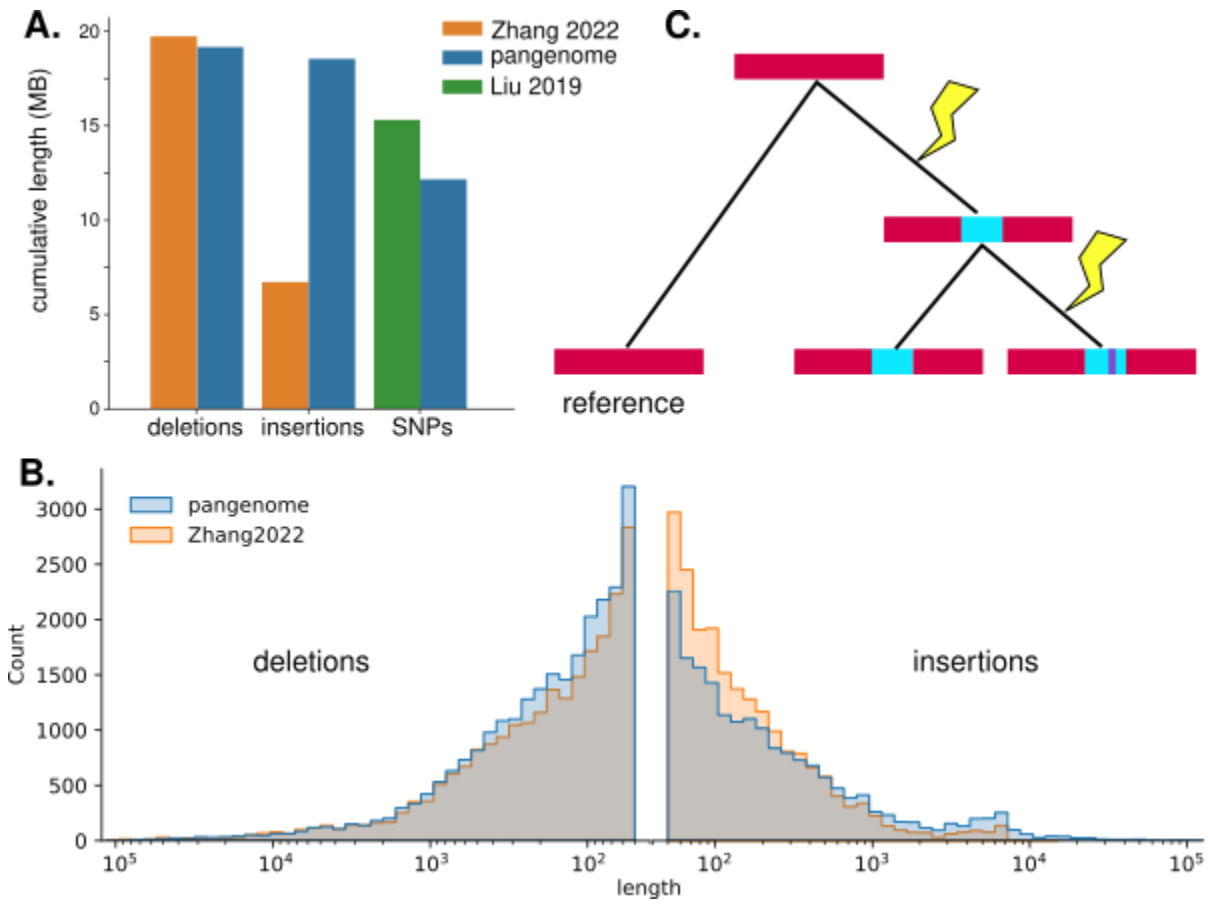

Figure 1: Cataloging variation in the pangenome graph. (a) Total lengths of sequence contained in insertions (INS), deletions (DEL), and SNVs, compared between this study ("pangenome") and read-alignment methods [41,42]. (b) Distribution of lengths of insertions and deletions found in this study compared to those found by Zhang et al. [41] using long reads shows that while long-read alignment finds more short insertions (< 1kb) than the pangenome, the larger cumulative length of insertions found by our pangenome compared to Zhang as shown in (a) is driven by long insertions (>1kb), which have a larger effect on cumulative length. (c) A hypothetical schematic of how nested variation can evolve: an insertion mutation is followed by a later single nucleotide mutation, resulting in an insertion relative to the reference that contains a segregating site. A genotype against a linear

819 reference would represent these as three different alleles, whereas a pangenome conserves the nested

820 structure of this variation.

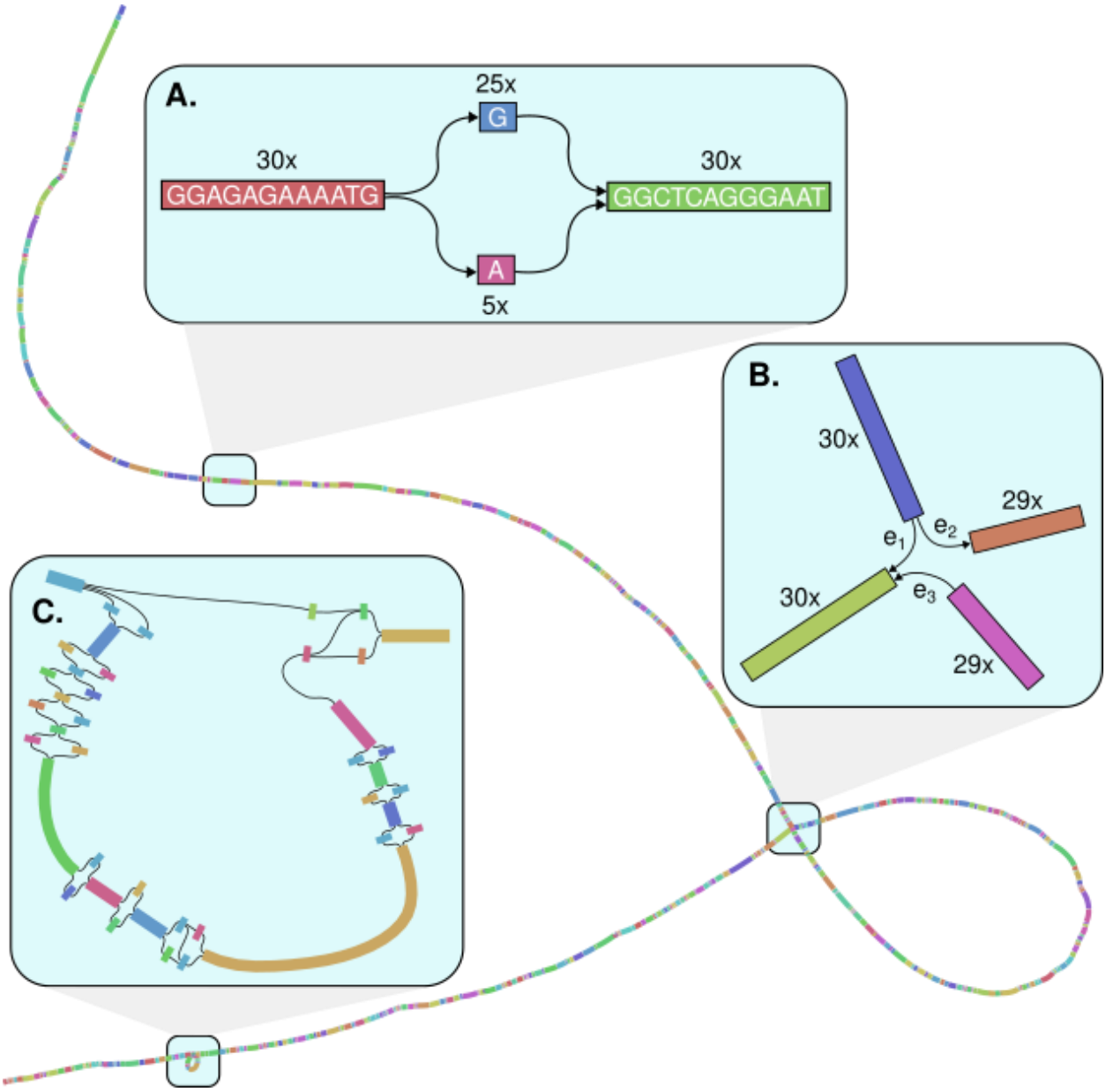

Figure 2: A visual representation of the pangenome graph for the gene *IGLL1*. (a) *IGLL1* contains many SNVs, including one at bGalGal1b#chr15:7,955,357, in its coding sequence. The graph of this SNV shows that while all 30 haplotypes have the same sequence before and after the SNV, 25 haplotypes have G in this position and 5 have A. (b) The pangenome of *IGLL1* contains a ~5kb deletion compared to bGalGal1b in one haplotype of a single individual, UCD312. At the

828 juncture in the pangenome graph where the deletion haplotype branches from the rest, this haplotype
829 follows edge e1 to skip the sequence in the loop, while the other 29 haplotypes follow edge e2 to
830 include the sequence, and then e3 to join back with the deletion haplotype afterwards. (c) *IGLL1* also
831 contains a ~300bp insertion compared to bGalGal1b in 22 haplotypes. The inserted sequence contains
832 SNVs, so while a linear representation of this insertion considers each version of the insertion as a
833 different allele, the pangenome graph is able to correctly record it as a biallelic variant (i.e., insertion or
834 no insertion) containing additional variable sites. Furthermore, reads can align to this sequence in the
835 pangenome but would be left unmapped when aligning to bGalGal1b as it does not contain this
836 sequence.

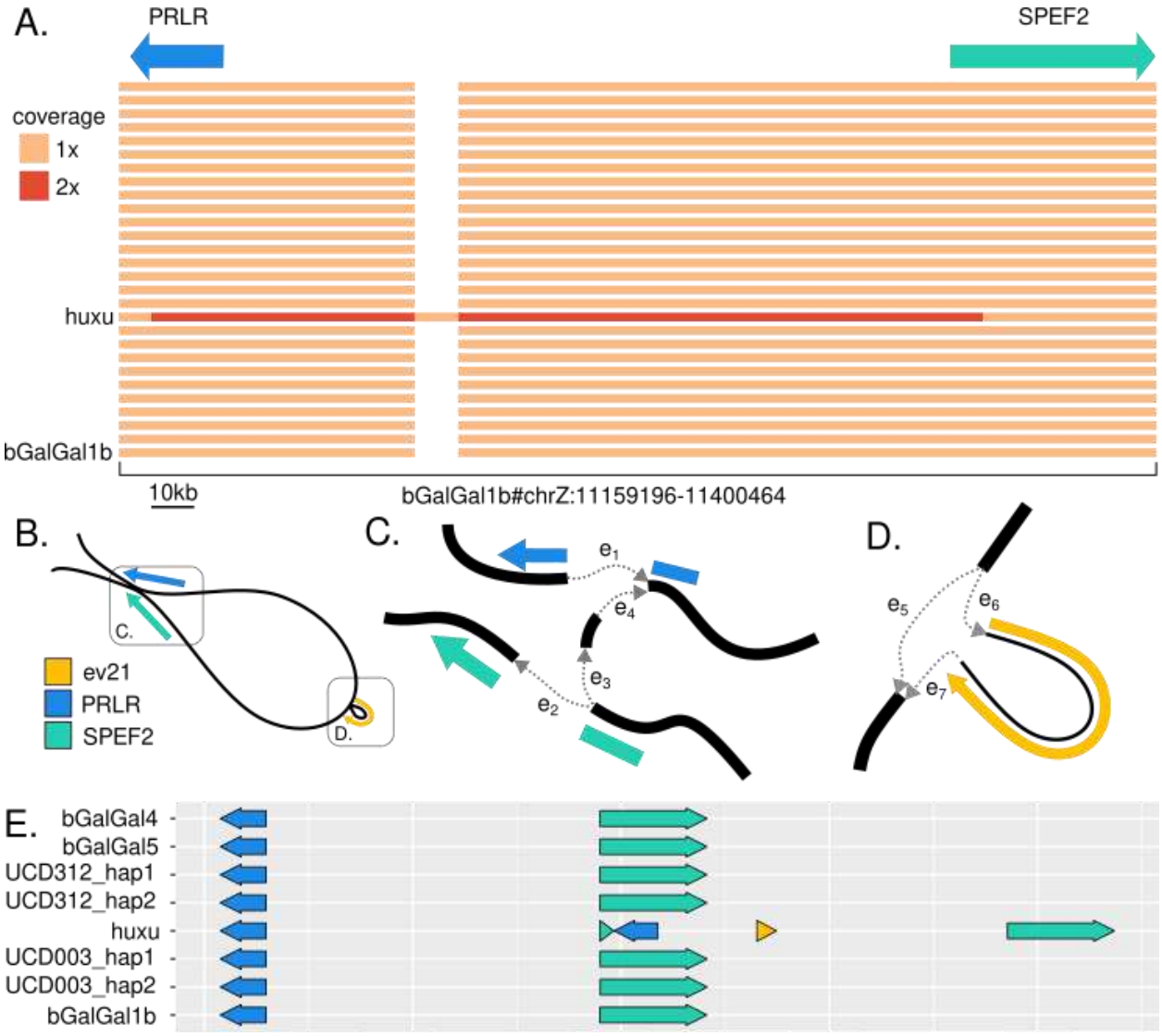

Figure 3: Disentangling complex variation at the K locus with the pangenome graph. (a) A one-dimensional view of the pangenome subgraph for the K locus, with nodes colored by path coverage (i.e., the number of times a haplotype path passes through them) and the locations of the genes *PRLR* and *SPEF2* denoted. Huxu shows double path coverage of part of the locus, as well as an insertion. Alignment verified that this insertion contains the sequence of the avian leukosis virus ev21. (b) A two-dimensional view of the same graph, showing both the tandem duplication and the ev21 insertion. (c) At the junction where the paths containing the tandem duplication deviate from the

paths that do not, all paths begin by traversing edge e1 and moving through most of the sequence of the K locus. However, at the e2/e3 fork, a path can either traverse e2 to leave the K locus, or traverse e3 and e4 to include a tandem duplication of parts of *PRLR* and *SPEF2*. (d) A more detailed view of the ev21 insertion, showing the two possible paths at this juncture: a path can traverse edge e5 to skip the insertion, or it can traverse edge e6, then the ev21 sequence, then e7, to include the insertion. (e) Linear untangled view of the locus, confirming previous studies of the structure of the locus, with a tandem duplication of parts of both genes and an insertion of the ev21 sequence.

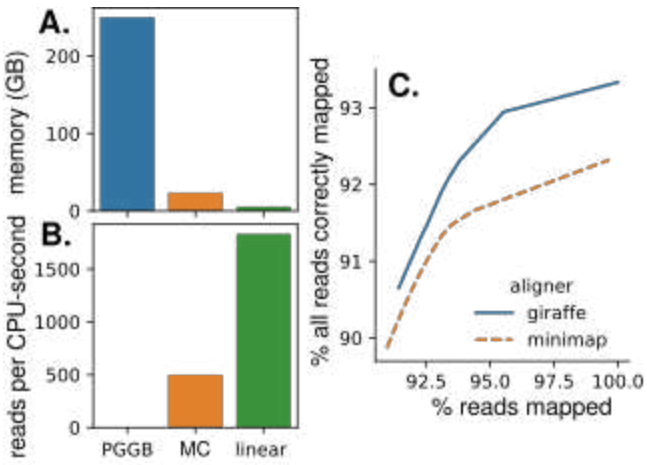

852

853 **Figure 4: Comparing pangenome and linear aligner performance for short reads.** (a-b)

854 Alignment of short reads with VG giraffe is more memory-efficient (a) and faster (b) when aligning to

855 the minigraph-cactus (MC) pangenome graph compared to the PGGB graph. Linear alignment with

856 minimap2 is the fastest and most memory-efficient. (c) A larger percentage of all simulated reads is

857 correctly aligned with giraffe regardless of how permissive the minimum map quality filter is.

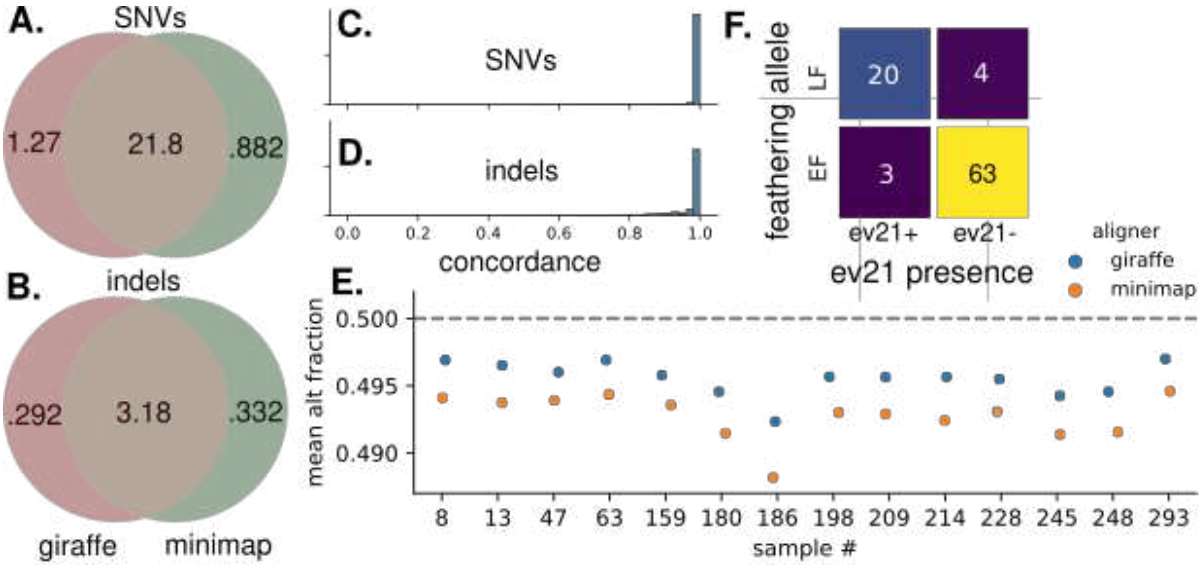

Figure 5: Genotyping 100 diverse chickens. (a-b) Counts in millions of common and different SNVs (a) and indels (b) found by genotyping pipelines using giraffe vs. minimap as the aligner. Only variants with a quality score of at least 10 are considered. (c-d) Concordance distributions for SNVs (c) and indels (d) detected by both genotyping methods with QUAL>=10. (e) Mean fractions per sample of mapped reads containing the alternate allele at putative heterozygous sites show that giraffe alignments contain less reference bias for every chicken, as they deviate less from the expected value of 0.5. Sample information in Supplementary Table 2 and full plot for all 100 chickens in Supplementary Figure S5. (f) Genotyping 100 chickens at the K locus reproduces previous results finding that while most chickens with the late feathering allele (LF) also have an ev21 insertion at the K locus (ev21+), some chickens have the late feathering allele without an ev21 insertion.

Supplementary Files

This is a list of supplementary files associated with this preprint. Click to download.

- Supplementarymaterial.docx